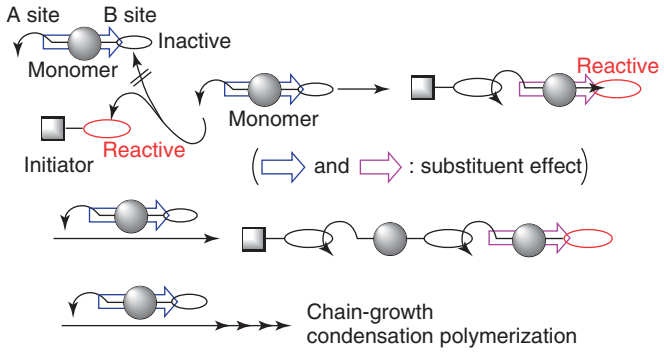

Figure 3.24 Scheme of chain-growth condensation polymerization. *Source*: Reprinted with permission from Yokoyama A, Yokozawa T. *Macromolecules* 2007;40:4093 [73]. Copyright 2007 American Chemical Society.

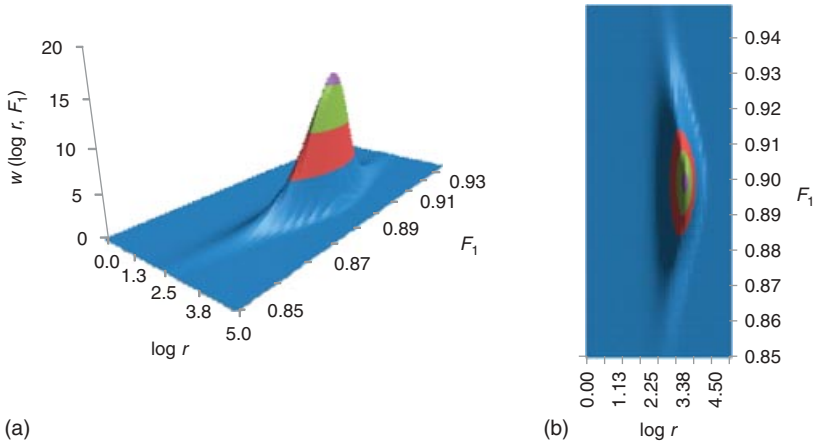

Figure 5.10 The Stockmayer distribution for a copolymer made with a single-site catalyst. (a) Three-dimensional plot, (b) Bird's eye view.

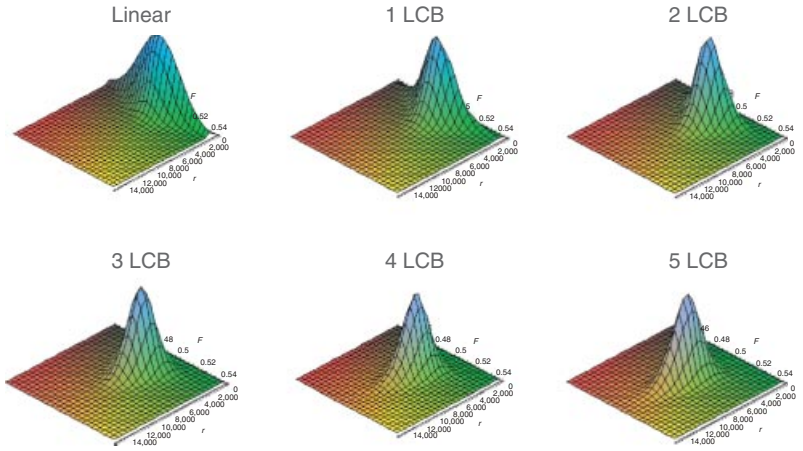

Figure 5.11 Trivariate distribution for a model polymer.

Handbook of Polymer Synthesis, Characterization, and Processing, First Edition. Edited by Enrique Saldívar-Guerra and Eduardo Vivaldo-Lima.

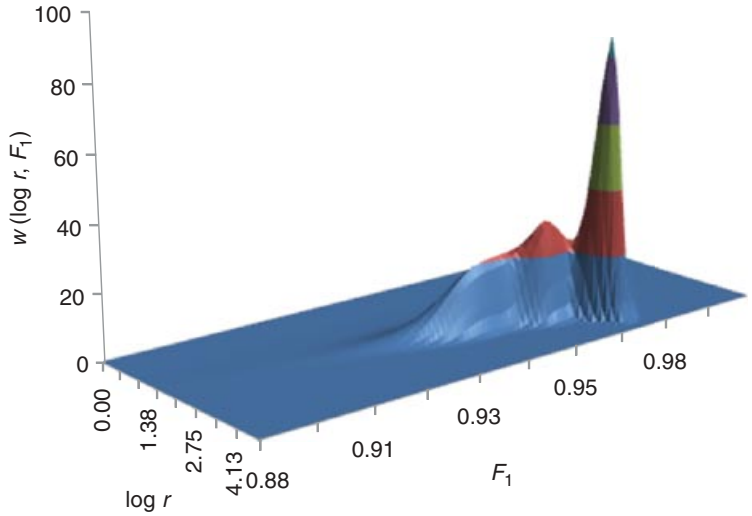

Figure 5.12 Simulated chain length and chemical composition distributions of a polymer made from a three-site catalyst.

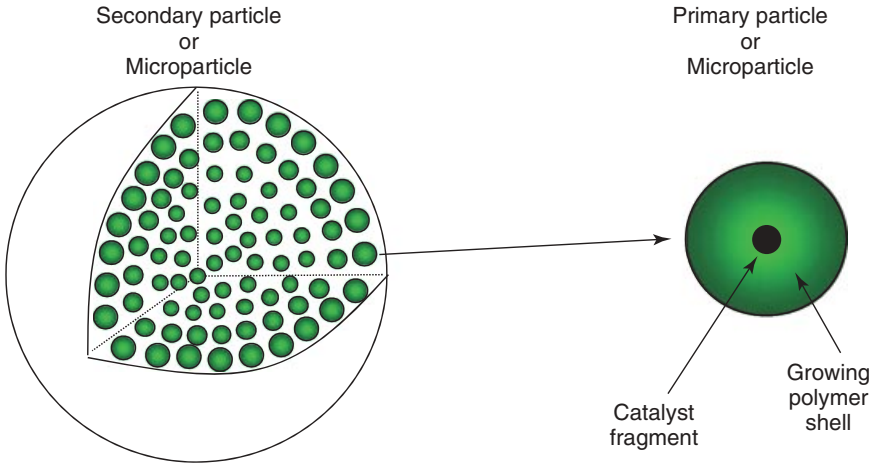

Figure 5.13 The multigrain model (MGM).

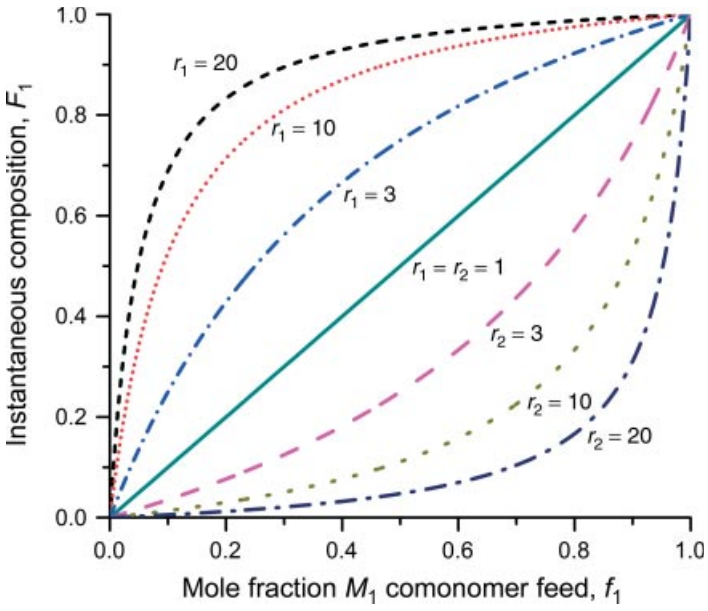

Figure 6.6 Dependence of instantaneous copolymer composition F_1 on initial comonomer feed composition f_1 in an ideal copolymer. The reactivity ratios satisfy $r_1 r_2 = 1$.

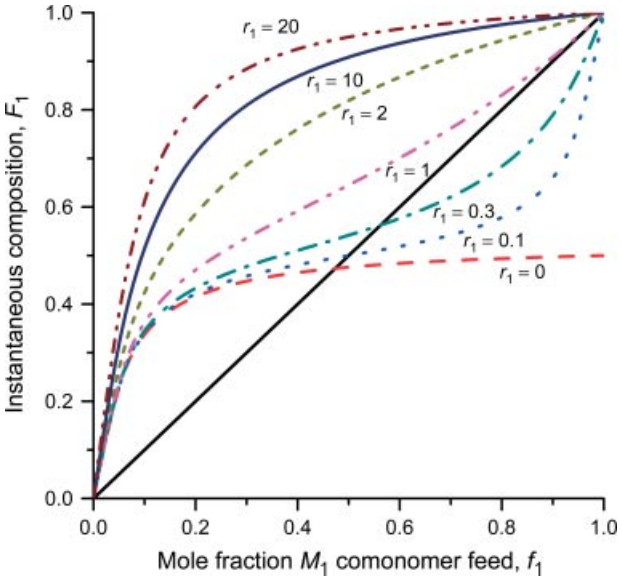

Figure 6.8 Dependence of instantaneous copolymer composition F_1 on initial comonomer feed composition f_1 for different values of r_1; $r_2 = 0.1$.

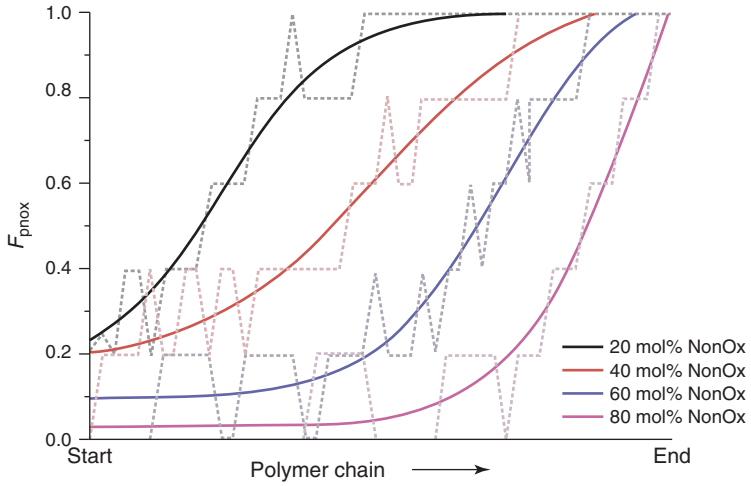

Figure 8.4 Monomer distribution along the polymer chain for statistical copolymers of 2-nonyl-2-oxazoline (NonOx) and 2-phenyl-2-oxazoline (PhOx). *Source*: Reprinted with permission Lambermont-Thijs HML, Jochems MJ, Hoogenboom R, Schubert US. J Polym Sci A Polym Chem 2009;47:6433 [176]. Copyright 2009 John Wiley and Sons, Inc.

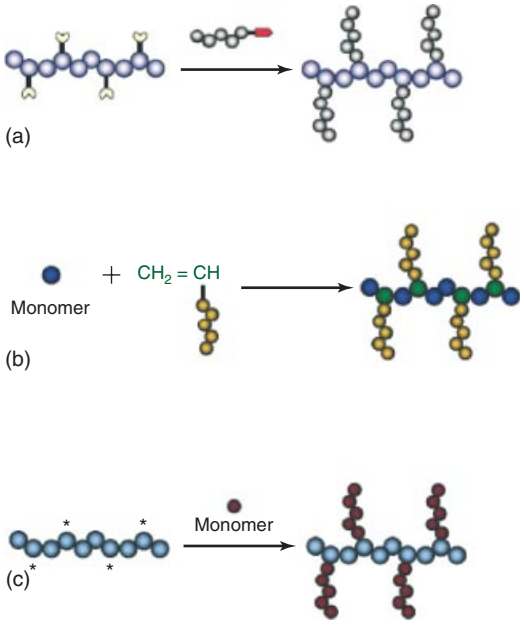

Figure 10.1 Schematic representation of (a) grafting-onto, (b) grafting-through, and (c) grafting-from methods.

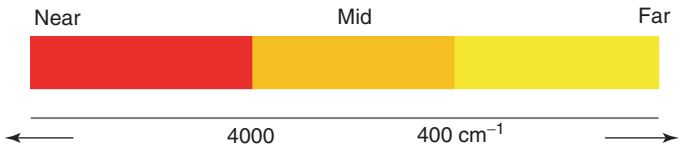

Figure 16.3 Regions for the study of IR: near, middle, and far.

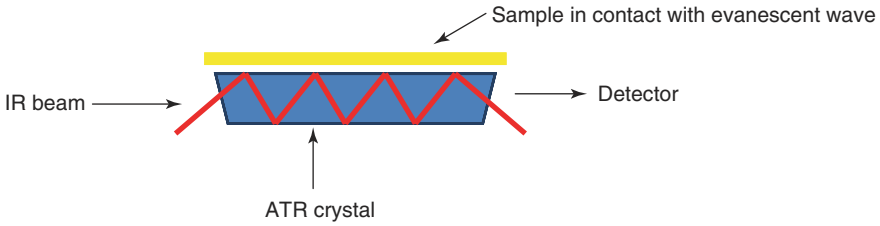

Figure 16.4 Mechanism of IR analysis by attenuated total reflectance.

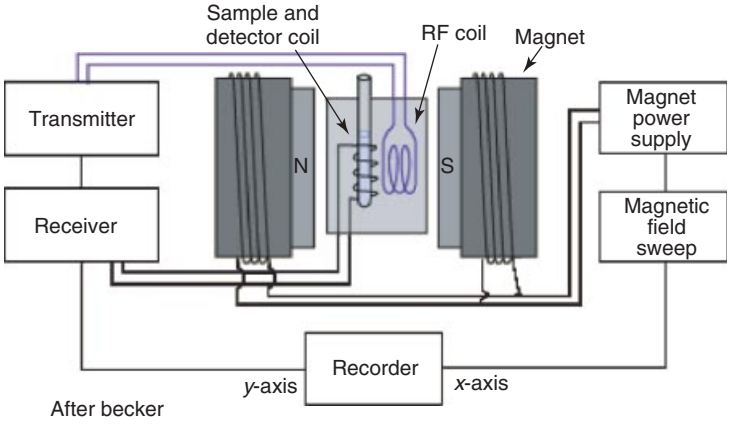

Figure 16.11 Diagram of an FT-NMR spectrometer.

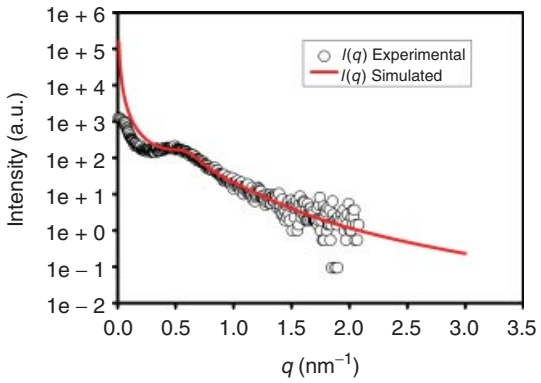

Figure 19.A.1 Intensity plot.

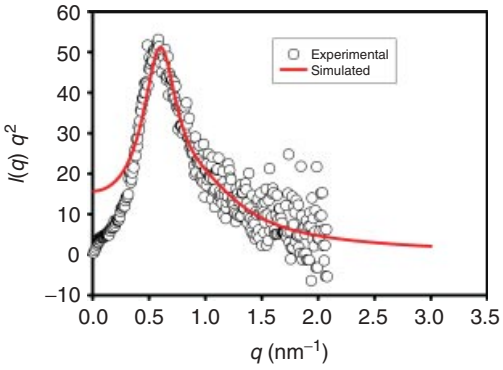

Figure 19.A.2 The Lorentz plot.

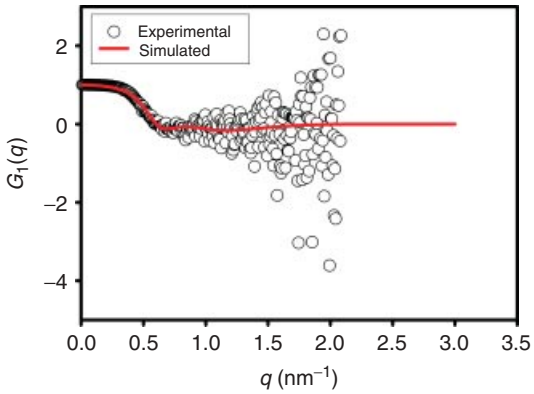

Figure 19.A.3 Interference function.

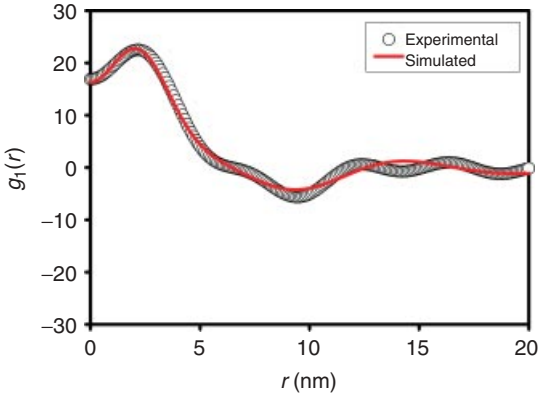

Figure 19.A.4 Interface distribution function.

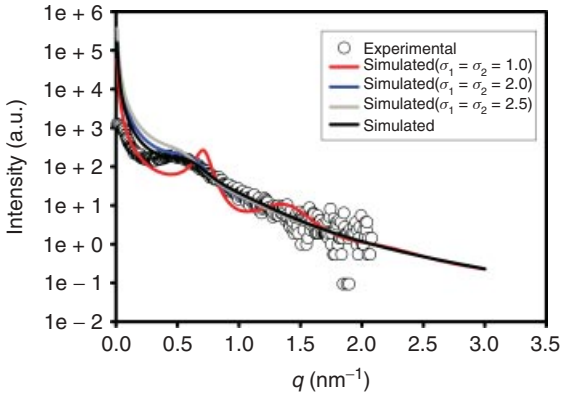

Figure 19.A.5 Statistical effect on the intensity plot.

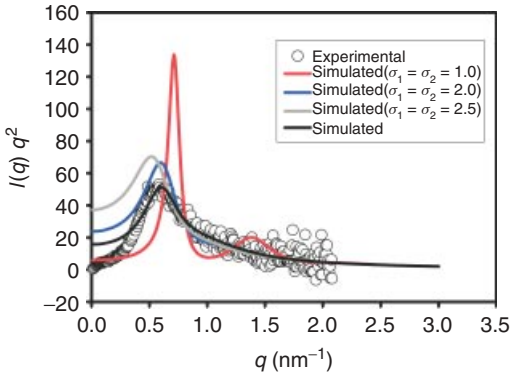

Figure 19.A.6 Statistical effect on the Lorentz plot.

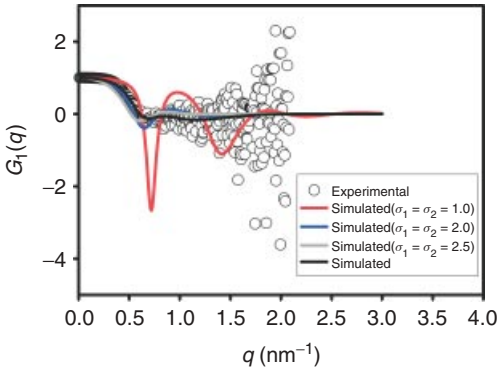

Figure 19.A.7 Statistical effect on the interference function.

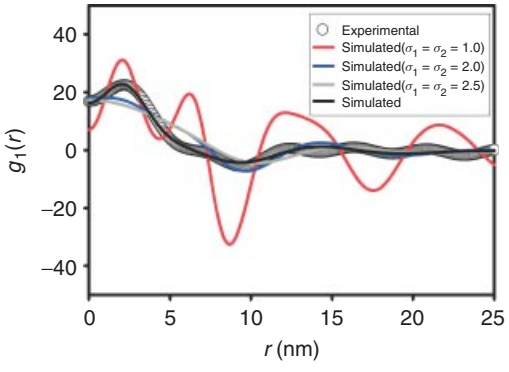

Figure 19.A.8 Statistical effect on the interface distribution function.

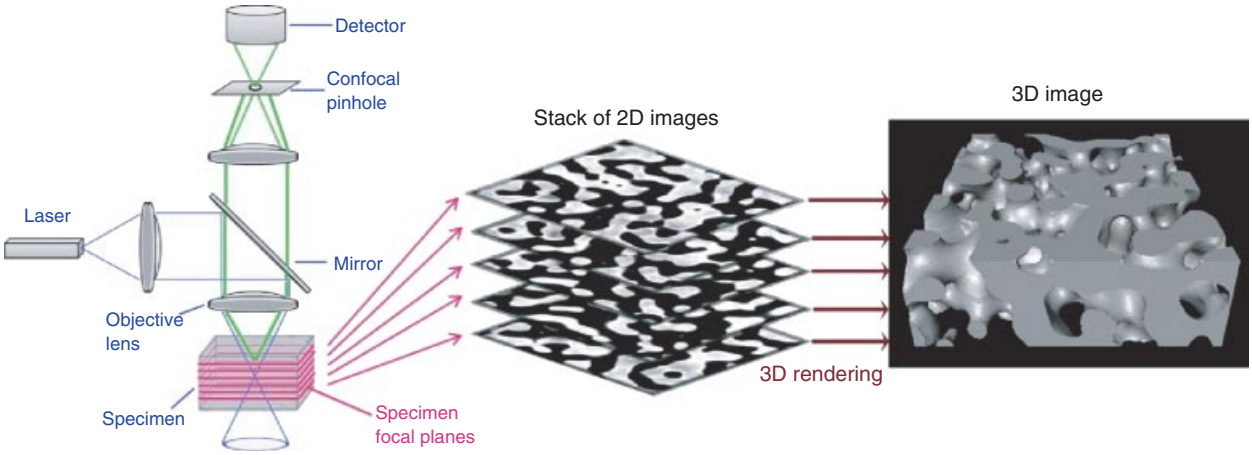

Figure 20.1 Schematic of LSCM. A stack of 2D images is recorded at different focal planes in the specimen and subsequently reconstructed in three dimensions using the marching cubes algorithm [136].

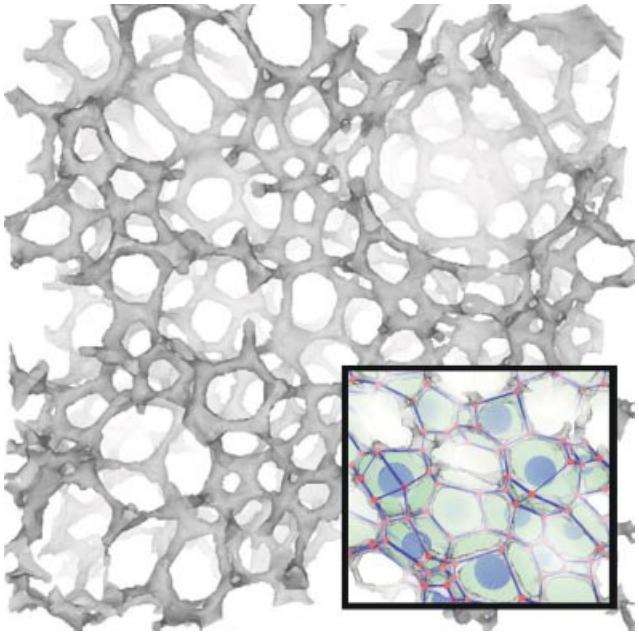

Figure 20.2 3D-rendered image of a polyurethane foam obtained via X-ray μ-CT. The black voxels within this image represent the locations of foam struts, while the white areas represent void space. The inset show a close-up of the foam structure showing the correlation between the detected strut, vertex, and cell locations and the original foam volume. The large blue spheres in the image indicate the centers of detected foam cells. *Source*: Reprinted with permission from Journal of Colloid and Interface Science, Vol. 280, M.D. Montminy, A.R. Tannenbaum, C.W. Macosko, The 3D structure of real polymer foams, Journal of Colloid and Interface Science 2004, 280, pages 202–211 [152]. Copyright 2004 Elsevier.

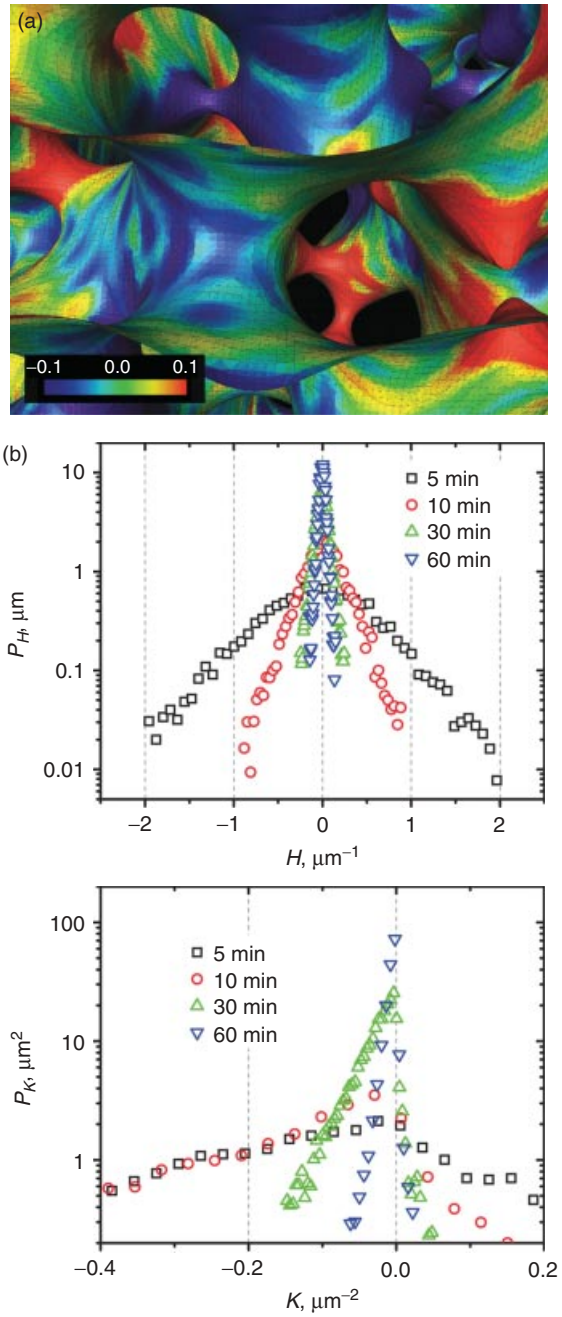

Figure 20.4 (a) 3D-rendered interface of 50/50 PS/SAN cocontinuous blend. The color in each triangle represents the value of the mean curvature given by the color bar scale. *Source*: Reproduced with permission from López-Barrón C, Macosko CW. A new model for the coarsening of cocontinuous morphologies. *Soft Matter* 2010;6:2637–2647 [149]. Copyright 2010 The Royal Society of Chemistry. (b) Probability densities of the mean and the Gaussian curvatures of the 50/50 PS/SAN interface at different annealing times. *Source*: Reprinted with permission from Lopez-Barron C, Macosko CW. Characterizing interface shape evolution in immiscible polymer blends via 3D image analysis. *Langmuir* 2009;25:9392–9404 [148]. Copyright 2009 American Chemical Society.

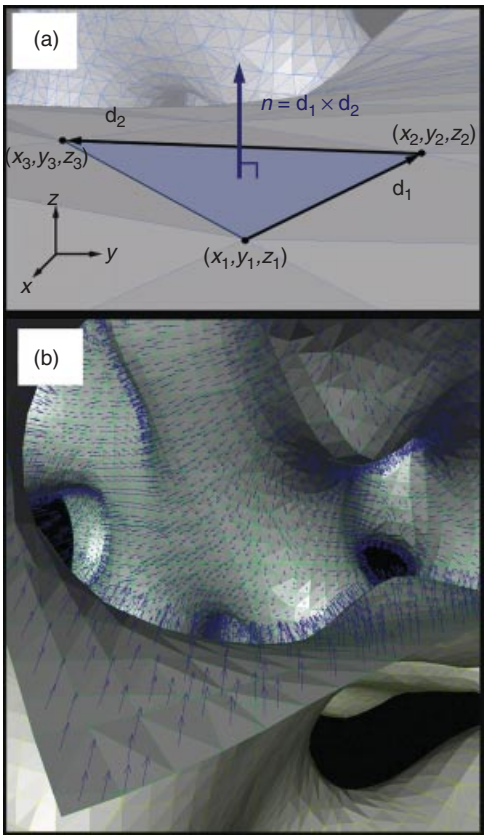

Figure 20.6 (a) Schematic of the computation of the vector normal to a triangle. (b) Detail of the normal vector field generated with the LCPM on a cocontinuous interface. *Source*: Reprinted with permission from López-Barrón CR, Macosko CW. Direct measurement of interface anisotropy of bicontinuous structures via 3D image analysis. *Langmuir* 2010;26 (17):14284–14293 [150]. Copyright 2010 American Chemical Society.

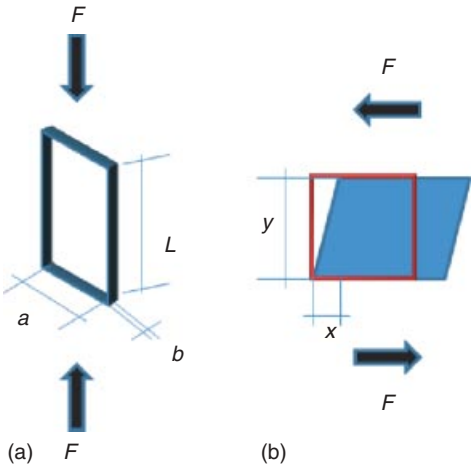

Figure 21.3 Common force fields for applied forces in a material (a) tension and (b) shear.

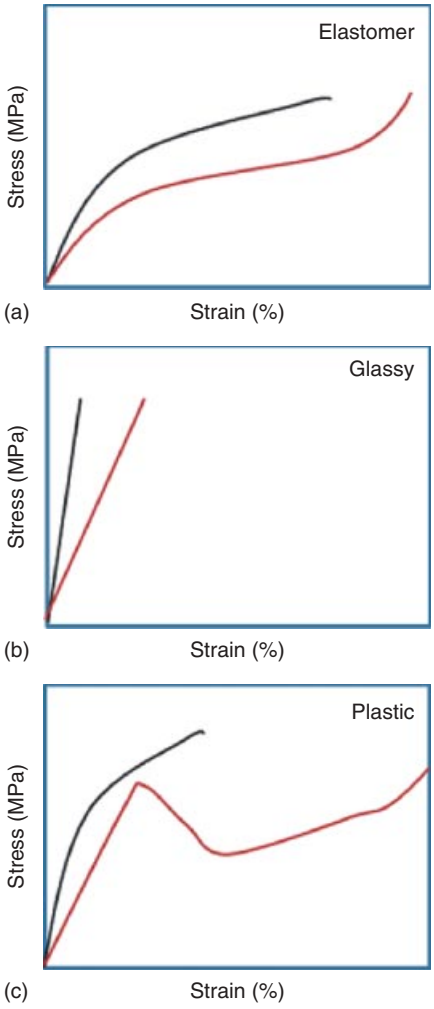

Figure 21.4 Typical stress-strain curves for different types of polymers: (a) elastomer, (b) glassy, and (c) plastic.

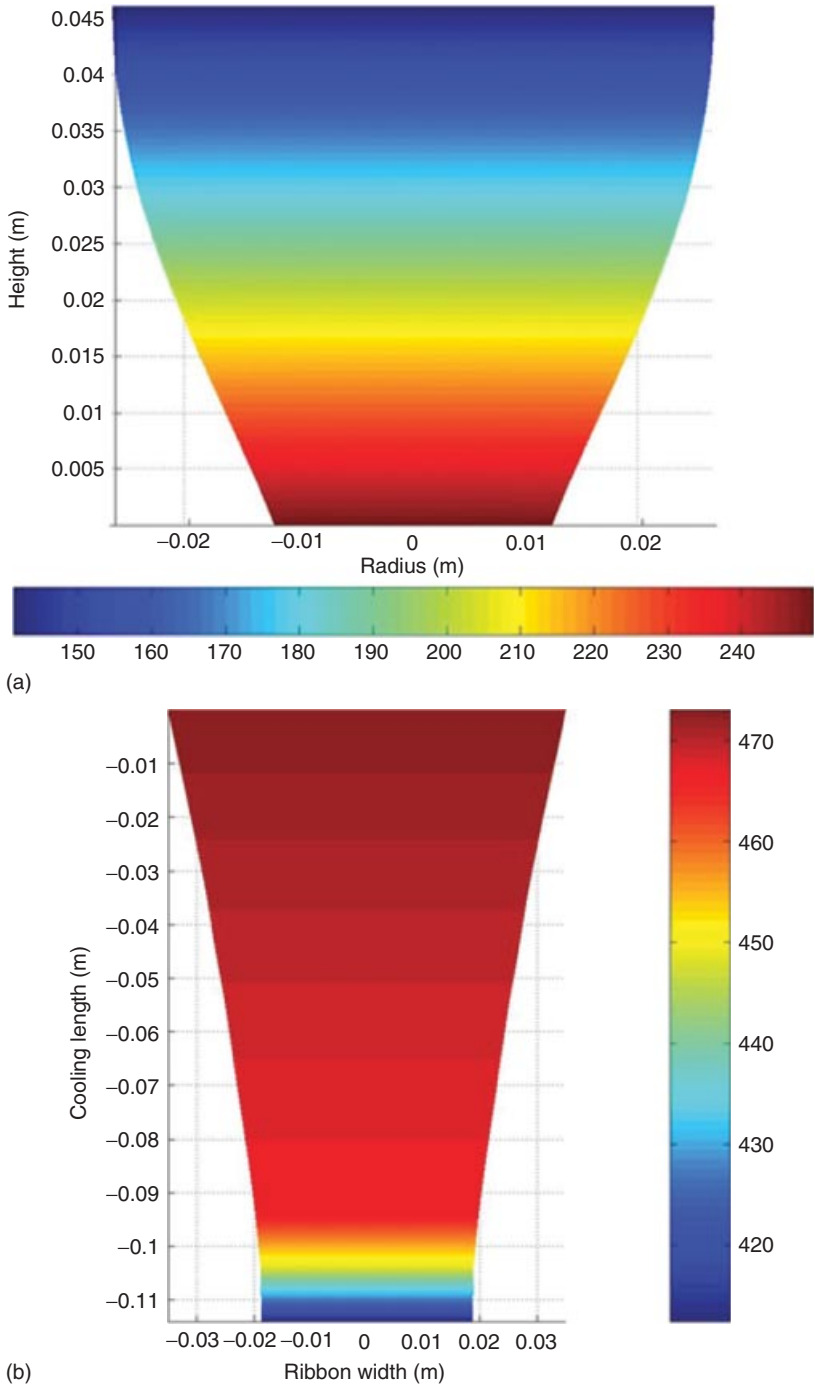

Figure 24.3 Simulated (a) bubble radius, (b) ribbon width, and temperature profiles.

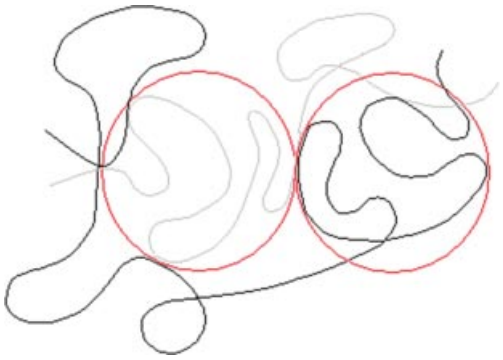

Figure 25.6 Representation of blobs in a polymer chain.

Figure 26.1 Typical composite components: (a) fiber, (b) polymer and additives.

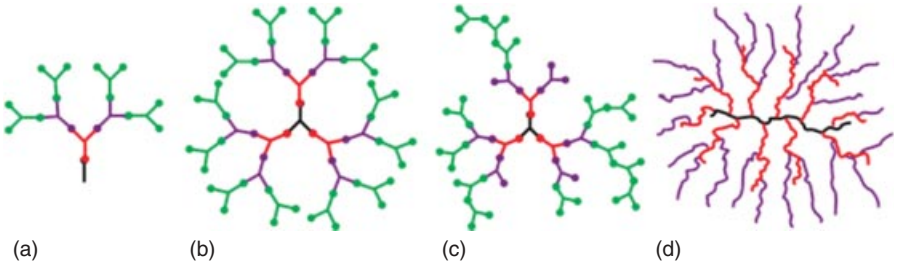

Figure 30.1 Structure of four types of dendritic polymers: (a) dendron, (b) dendrimer, (c) hyperbranched polymer, and (d) dendrigraft polymer.

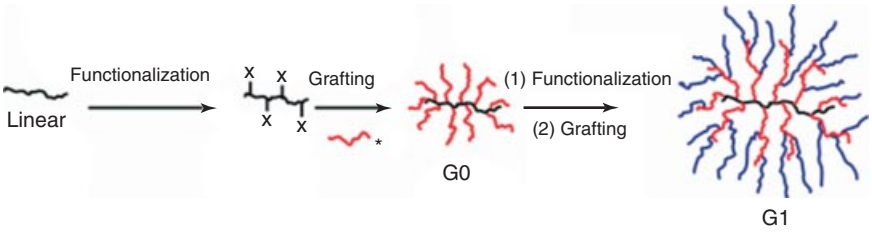

Figure 30.9 Schematic representation of the generation-based synthesis of dendrigraft polymers by a divergent *grafting-onto* method.

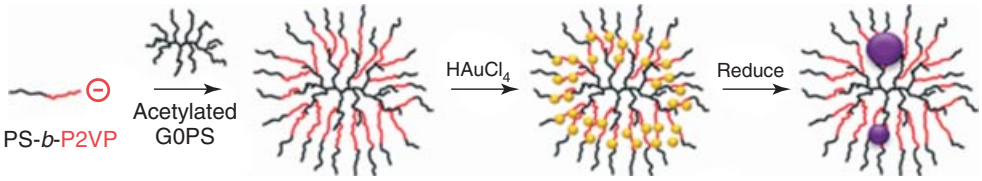

Figure 30.11 Synthesis of an arborescent copolymer, G0PS-*g*-(P2VP-*b*-PS), its application to templating $HAuCl_4$ deposition, and reduction to gold nanoparticles.

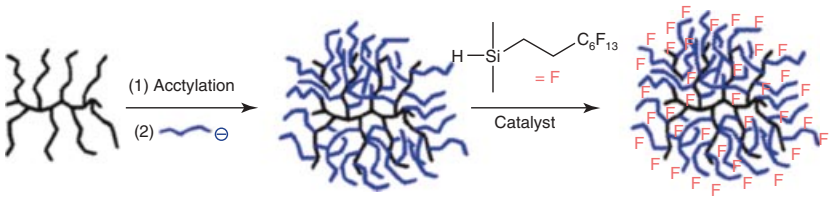

Scheme 30.19 Synthesis of G0PS-*g*-PIP copolymer followed by hydrosilation with a fluorohydrosilane for use as a processing aid. *Source*: Reproduced with permission from Gauthier M, Lin W–Y, Teertstra SJ, Tzoganakis C. Polymer 2010;51:3123 [121]. Copyright 2010 Elsevier.